European Journal of Mechanics / B Fluids 82 (2020) 156–160

Contents lists available at ScienceDirect

European Journal of Mechanics / B Fluids

journal homepage: www.elsevier.com/locate/ejmflu

An analytic solution for bottom intensified flow along sloping topography

Joseph Kuehl *, Charles McMahon

University of Delaware, Department of Mechanical Engineering, 130 Academy Street, Newark, DE 19716, USA

ARTICLE INFO

Article history:
Received 16 October 2019
Received in revised form 9 February 2020
Accepted 24 March 2020
Available online 3 April 2020

Keywords:
Analytic solution
Similarity solution
Topographic control
Western boundary current

ABSTRACT

A self-similar nonlinear analytic solution is derived for a case of isolated deep flow over broad sloping topography. The solution takes the form of an arctangent function and physically manifests as a compressing jet (narrowing and intensifying) with Ekman pumping controlling the interface evolution. Notably, this jet travels in the direction with shallow water to the left, which is in contrast to the expected flow direction of topographic Rossby wave propagation (shallow water to the right). Such deep flows are not accessible via satellite observations and play an important role ocean-coastal ocean connectivity. Examples of deep flows over broad shelves include the South Atlantic Bight and West Florida Shelf, where deep upwelling is thought to influence the generation of red tides, local ecosystems, and deep carbon sequestration. Relevance of the analytic solution to the South Atlantic Bight circulation is provided.

1. Introduction

The objective of this manuscript is to gain insight into the fundamental physics of an important class of layered ocean system: isolated deep circulations over sloping topography (relevant to shelf and slope dynamics). While this case is accessible to investigation by direct numerical simulation, here we choose an analytic approach to isolate particular physics. It should be emphasized that an important utility of such analytic results is that they provide a fundamental framework upon which further analysis can be conducted (e.g. higher order analytic extensions, stability analysis). Additionally, analytic solutions can assist in the interpretation of observational and numerical data sets. For example, consider the lasting impact of works such as [1] and [2] which, while considered basic by modern computationally driven standards, continue to greatly influence fluid dynamics communities.

The case considered is a study of deep subsurface flow along broad continental shelves and slopes. Such flows are invisible to satellite observation as they have no surface expression. However, they may have significant implications for shelf and slope ecosystems, open-coastal ocean connectivity, and global carbon sequestration. Though we make no direct comparison with observational current data here, examples of broad continental shelves and slopes include the West Florida Shelf (WFS) and South Atlantic Bight (SAB). Deep upwelling flow on the WFS is thought to lead to red tide phenomena and the transport of hazardous materials [3–5]. Gulf Stream interaction with the broad SAB shelf leads to upwelled water masses that are important for local ecosystems [6] and may be significant pathways for carbon sequestration [7]. While these examples provide motivation for studying such systems, the treatment here is purely analytic and is formulated as an idealized rotating fluid basin with sloping topography. Later, in Section 5, application of the solution to the SAB is discussed.

This manuscript is organized as follows. In Section 2, we discuss the problem formulation in the context of a rotating table laboratory experiment. In Section 3, we derive the relevant vorticity equation which describes the dynamics of bottom intensified flow along a sloping topography and solve the equation analytically. Section 4 is a discussion of the results and Section 5 discusses application of the solution to the SAB.

2. Problem formulation

We formulate the problem of layered oceanographic flow in the context of a two-layer rotating table experiment. Consider a square rotating tank (with dimensions of approximately 1 meter) in which a two fluid layers are contained between a sloping rigid-lid and sloping bottom (Fig. 1). Such a setup serves as a convenient model for the study of idealized ocean dynamics. The rotation of the platform creates a Coriolis effect which, in conjunction with the sloping rigid-lid and sloping bottom, induces a topographic β-effect in each layer. Each layer also has a specified density (ρ_i) and depth (h_i). The layer depth can further be decomposed as $h_i = h_{0i} + h_{bi} + \eta_i$, where h_{0i} is the mean layer depth, h_{bi}

* Corresponding author.
E-mail address: jkuehl@udel.edu (J. Kuehl).

https://doi.org/10.1016/j.euromechflu.2020.03.007
0997-7546/

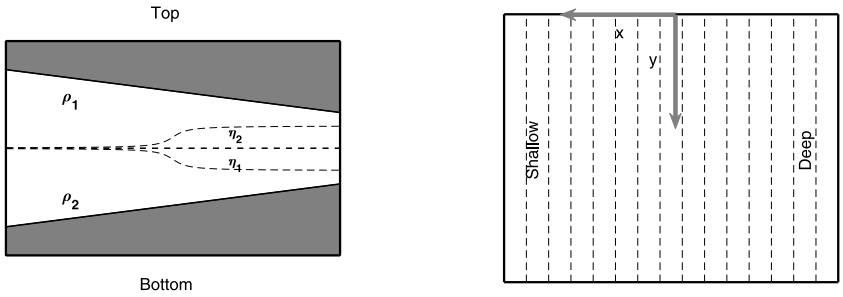

Fig. 1. Two-layer rotating fluid tank setup. Left: Side view of two-layer system with sloping lid and bottom shown along with interfacial displacement sense for each case. Right: Top view of Case A. Dashed lines are isobaths.

is the topographic variation, and η_i is the interface displacement relative to no motion. It is important to note that the upper-layer interface displacement (η_1) is positive downwards and the lower-layer interface displacement (η_2) is positive upwards. The right panel of Fig. 1 illustrates the coordinate system and flow orientation relative to isobaths (indicated by dashed lines). The flow will primarily be along the topography. Later it will be shown that at $y = 0$, a step function boundary condition on transport is applied and the flow diminishes as $x \to \pm\infty$.

This work considers a 1.5-layer system in which the upper-layer is assumed to be quiescent. That is, the flow is concentrated in the lower-layer with a negligible upper-layer flow. Following the work of Zavala Sanson and van Heijst [8], the momentum equations and continuity equation for the single active fluid layer are:

$$\begin{aligned} u_t - (f+\omega)v &= -(p+e)_x + \nu\nabla^2 u \\ v_t + (f+\omega)u &= -(p+e)_y + \nu\nabla^2 v \\ h_t + (hu)_x + (hv)_y + \nabla\cdot\Pi_E &= 0. \end{aligned} \tag{1}$$

The layer identifying subscripts have been dropped as Eq. (1) are valid for either layer. Details can be found in [9] or, in particular, the [10] chapter on layered systems. More explicitly, [11] provide the coupled two-layer system set of equations. Eq. (1) result from simply taking the 1.5-layer limit and noting the above mentioned sense of interface displacement.

In Eq. (1): u, v are the cross-slope and along-slope velocities, respectively, h is the depth of the fluid layer, $e = (u^2+v^2)/2$ is kinetic energy per unit mass, $\omega = v_x - u_y$ is the vorticity, ν is the viscosity, f is the Coriolis parameter, and p is the pressure anomaly relative to no motion, divided by the fluid density (ρ). As this work considers layered systems, p can also be interpreted as the Montgomery Potential. Either way, $p = g'h$ is obtained, where $g' = (\Delta\rho/\rho_1)g$ is the reduced gravity, and $\Delta\rho = \rho_2 - \rho_1$. The effect of the viscous bottom boundary layer is accounted for by a small correction term $\vec{\Pi}_E = \frac{1}{2}h_E\hat{\mathbf{k}}\times\vec{u}$, the Ekman flux. Its divergence, $\nabla\cdot(\vec{\Pi}_E) = -\frac{1}{2}h_E\omega$, represents first-order Ekman suction at a solid boundary with Ekman layer depth, $h_E = \sqrt{2\nu/f}$. Taking the curl of the momentum equations, defining an interior transport function (ψ) through $h\mathbf{u} = \hat{k}\times\nabla\psi + \nabla\phi$ (where $\nabla^2\phi = -\nabla\cdot\Pi_E = \frac{1}{2}h_E\omega$ represents Ekman divergence), and simplifying by letting $q = \frac{f+\omega}{h}$ gives us the steady state vorticity-transport equation,

$$J(\psi,q) + \nabla\phi\cdot\nabla q = -\frac{h_E}{2}q\omega + \nu\nabla^2\omega. \tag{2}$$

It is the intention of this manuscript to consider steady state solutions, and the steady state assumption was implicitly made to obtain $\nabla^2\phi = -\nabla\cdot\Pi_E$. Note that $\nabla\phi = \frac{1}{2}\frac{h_E}{h}\nabla\psi$, which can be obtained from combining the definition of the transport function with the Ekman dissipation and expanding in the assumed small term $\frac{h_E}{h}$ [12].

3. Bottom intensified flow along a sloping topography

We now seek a solution to the equations of motion that govern bottom intensified, weak flow along a broad shelf or slope. Again, this situation is depicted in Fig. 1, and the flow is assumed to primarily follow the topography (±y-direction) with shallow water in the positive x-direction. Beginning with Eq. (2), a series of approximations are made to further reduce the equation into an analytically tractable form.

- $\nabla\phi\cdot\nabla q \to 0$. Physically, this term represents the vorticity advection by the divergent component of the flow field. In the present case, this is the advection of vorticity by the boundary layer which is expected to be small. This can be seen by recalling $\nabla\phi = \frac{1}{2}\frac{h_E}{h}\nabla\psi$ and noting that the divergent component caused by the Ekman suction is small. For the laboratory case, $\phi/\psi = h_E/h = O(10^{-2})$ which justifies the approximation.
- $J(\psi,q) \to \frac{1}{h}J(\psi,\omega) + \frac{\beta^{(x)}}{h}\psi_y - \frac{\beta^{(y)}}{h}\psi_x - \frac{f}{h^2}J(\psi,\eta)$. This is accomplished by decomposing the lower-layer depth to $h = h_0 + h_b + \eta$, as described above. The Jacobian $J(\psi,q) = \psi_x q_y - \psi_y q_x$ may be expanded to $\frac{1}{h}J(\psi,\omega) - \frac{f}{h^2}J(\psi,h_b) - \frac{f}{h^2}J(\psi,\eta)$ with the assumption $\omega \ll f$. Assuming a linearly varying topography in the across-slope direction, the $-\frac{f}{h^2}J(\psi,h_b)$ term may be further expanded to $\frac{\beta^{(x)}}{h}\psi_y - \frac{\beta^{(y)}}{h}\psi_x$, where $\beta^{(x)} = (f/h)\partial h_b/\partial x$ and $\beta^{(y)} = (f/h)\partial h_b/\partial y$ are the average topographic beta-effects.
- $-\frac{f}{h^2}J(\psi,\eta) \to \frac{f}{h^2}\frac{f}{g'h}\psi_y\psi_x$. Across topography gradients are expected to dominate along topographic gradients so a semi-geostrophic balance of the form $\eta_x = \frac{f}{g'h}\psi_x$. Thus, $-\frac{f}{h^2}J(\psi,\eta) \approx \frac{f}{h^2}\psi_y\eta_x = \frac{f}{h^2}\frac{f}{g'h}\psi_y\psi_x$.

To this point, the approximations made have been fairly standard and Eq. (2) reduces to

$$\frac{1}{h}J(\psi,\omega) + \frac{\beta^{(x)}}{h}\psi_y - \frac{\beta^{(y)}}{h}\psi_x + \frac{f^2}{g'h^3}\psi_y\psi_x = -\frac{h_E}{2}q\omega + \nu\nabla^2\omega. \tag{3}$$

Two more standard approximations will now be made, in addition to a novel third approximation before we reach our final form.

- It will be assumed that Ekman friction is dominant over lateral friction. Because there is weak shear in the flow and no lateral boundaries, the horizontally boundaries (layer interface and bottom) will dominate the frictional effects.
- It has been assumed above that along-slope flow is expected in which the cross-slope gradients are dominant over along-slope gradients. A consequence of which is that $\omega \approx \frac{1}{h}\psi_{xx}$.
- Finally, we seek a scaling in which the nonlinear advection of vorticity is neglected, but interfacial advection remains. By considering the relevant terms, it is seen that

this condition is satisfied if the across-slope length scale is large compared to the internal Rossby radius of deformation $\left(L^2 \gg L_D^2 = \frac{g'h}{f^2}\right)$.

Thus, the governing equation for bottom intensified, weak flow along a broad shelf or slope is

$$(h_b)_x f\psi_y - (h_b)_y f\psi_x + \frac{f^2}{g'h}\psi_y\psi_x = -\frac{h_E f}{2}\psi_{xx}. \tag{4}$$

3.1. Solution

Csanady [13] noted the similarity of Eq. (4), without the interfacial term (third term on LHS), to the heat equation. Following this note, [14] found that an analytic solution to this equation, without the interfacial term, takes the form of an error function. Kuehl's solution was extended to consider advective nonlinearities (i.e. vorticity advection described by Eq. (3) but without the interfacial term) by Ibanez et al. [15], who found an analytic solution that takes the form of a Lambert W function. Here, we will follow the same similarity solution approach adopted by Kuehl [14] and Ibanez et al. [15] to solve the nonlinear ordinary differential Eq. (4) analytically.

We begin by introducing the nondimensional transport function $\Phi = \frac{\psi}{Q}$ where Q is the total transport, a similarity variable of the form $\zeta = x(ky)^n$, and assume a sloping bottom topography of the form $h_b = -\alpha x y^{-\gamma}$, where k, n, γ, and α are constants to be determined. The relevant derivatives are

$$\Phi_y = \Phi'\frac{\partial\zeta}{\partial y} = knx(ky)^{n-1}\Phi' \tag{5}$$

$$\Phi_x = \Phi'\frac{\partial\zeta}{\partial x} = (ky)^n\Phi' \tag{6}$$

$$\Phi_{xx} = \left(\Phi'\frac{\partial\zeta}{\partial x}\right)_x = (ky)^{2n}\Phi'' \tag{7}$$

$$h_{by} = \alpha\gamma x y^{-\gamma-1} \tag{8}$$

$$h_{bx} = -\alpha y^{-\gamma}. \tag{9}$$

Upon substitution and simplification, Eq. (4) takes the form

$$-(\gamma+n)\alpha f y^{-(\gamma+1)}\zeta\Phi' + \frac{Q}{L_D^2}nk^n y^{n-1}\zeta\Phi'\Phi' = -\frac{h_E f}{2}(ky)^{2n}\Phi''. \tag{10}$$

Balancing the powers of y between each term in Eq. (10) yields the relationships $-(\gamma+1) = (n-1) = 2n$, which gives $n = -1$ and $\gamma = 1$. Ultimately, the system of equations becomes

$$\zeta\Phi'\Phi' = K_0\Phi'' \tag{11}$$
$$\zeta = k^{-1}y^{-1}x \equiv cxy^{-1}$$
$$h_b = -\alpha x y^{-1}$$
$$K_0 = \frac{L_D^2 h_E f}{2kQ} \equiv \frac{L_D^2 c h_E f}{2Q},$$

where $c = k^{-1}$ has been introduced for convenience. The resulting topography is shown in Fig. 2 (left). Upon substitution and separation of variables, Eq. (11) has an analytic solution which takes the form of an arctangent function,

$$\Phi = c_2 - \frac{2K_0}{\sqrt{2c_1}}\arctan\left(\frac{\zeta}{\sqrt{2c_1}}\right). \tag{12}$$

3.2. Boundary and spatial initial conditions

Coefficients c_1 and c_2 are determined by applying the boundary conditions that Φ varies between 0 and 1 as ζ varies between $\pm\infty$. The condition $\zeta \to -\infty$, $\Phi \to 1$ yields $c_2 = 1 - \frac{\pi K_0}{\sqrt{2c_1}}$. The condition $\zeta \to \infty$, $\Phi \to 0$ yields $0 = c_2 - \frac{\pi K_0}{\sqrt{2c_1}}$. Therefore, $c_1 = 2\pi^2 K_0^2$ and $c_2 = \frac{1}{2}$. Thus, the final solution is

$$\Phi = \frac{1}{2} - \frac{1}{\pi}\arctan\left(\frac{\zeta}{2\pi K_0}\right). \tag{13}$$

Assuming $y, c > 0$ and taking the limit as $y \to 0$ recovers the spatial initial condition at the singularity. Analytically, the solution is limiting to a step function in transport and a delta function in velocity flowing in the $-y$-direction. Taking the other limit, as $y \to \infty$, the solution is physically limiting to a broad uniform flow in the $-y$-direction of vanishing amplitude, as can be seen in Fig. 2 (right).

3.3. Layer interactions

The primary interaction between layers will be through interfacial Ekman pumping. This can be modeled by modifying the coefficient of the Ekman term with a scalar factor to account for interfacial Ekman effects. In the upper-layer equations of motion, the Ekman term will act as a forcing proportional to the magnitude of vorticity in the lower-layer. The solution derived above for lower-layer flow is both broad and weak, thus the magnitude of vorticity is small and the upper-layer will remain quiescent.

4. Discussion

Upon consideration of Eq. (4), it is readily observed that the derived solution is also valid over flat topography and for a barotropic fluid, given the scaling applies. However, the most interesting application is to isolated deep flow over sloping topography. Notably the flow is in the opposite direction to what is normally associated with motion along sloping topography. That is, currents along sloping topographies are most often thought to flow with shallow water to the right (consistent with topographic Rossby wave propagation). However, here we have shown that deep isolated currents can exist which flow with shallow water to the left. This behavior can be explained by considering the special form of the assumed topography (which is later shown to be relevant to the SAB). Notice that the topographic β-effect terms (first two terms on the LHS of Eq. (4)) cancel. These terms support topographic Rossby wave propagation with shallow water to the right. In their absence, a new fundamental balance is observed for the given scaling. Inspection of Eq. (11) reveals that the new balance is between interfacial advection term and the Ekman dissipation. In that equation, $\Phi'\Phi'$ is positive definite and $K_0 > 0$. When $\zeta < 0$ then $\Phi'' < 0$, and when $\zeta > 0$ then $\Phi'' > 0$, i.e. positive vorticity on the shallow side and negative vorticity on the deep side of the current. Physically, the current behaves as a compressing jet (narrowing and intensifying) in the flow direction ($-y$-direction). As the topography steepens, the current intensifies limiting towards a step function. As the solution approaches the singularity, the scaling breaks down and the domain of validity of the solution must be truncated, as discussed in [14] and [15]. Note that the similarity variable and depth variation (h_b) have a similar form, and thus the flow is predominantly along topography. This is in contrast to the barotropic solutions of Kuehl [14] and Ibanez et al. [15], in which Ekman dissipation cause cross isobath spreading of the topographically controlled current. Here, the Ekman pumping is directly tied to the evolution of the layer interface position, with the pumping allowing for the compression of the current in the $-y$-direction.

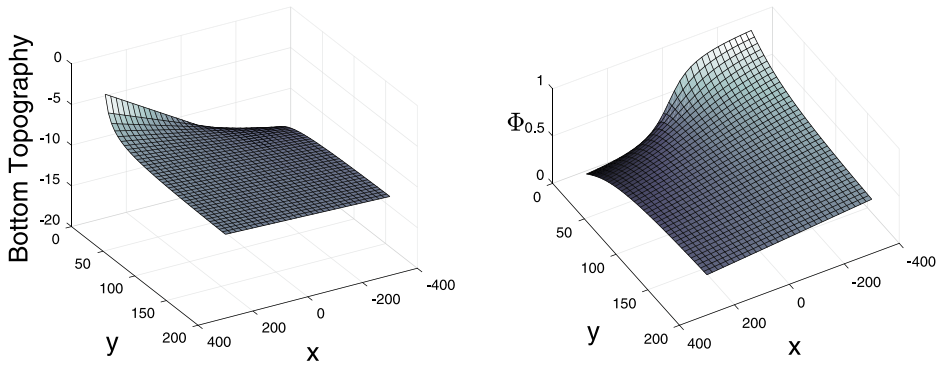

Fig. 2. Illustration of the stratified topographic β-plume solution, roughly scaled to that of a laboratory experiment (spatial dimensions in *cm*). Left panel shows typical bottom topography and right panel shows nondimensional transport function.

5. Application: South atlantic bight

While the analytic solution formulated above was cast in terms of rotating table laboratory experiments, the general problem was motivated by oceanographic regions such as the SAB and West Florida Shelf. Here we consider the topography of the SAB and discuss implications of our model to circulation in the region. Fig. 3 illustrates the topography of the SAB. In this region, a long (250 km+) and broad (≈75 km) shelf is observed. Numerics and observations in the region show, at times, a broad northward flow along the topography [16], which is particularly impactful to the fate of upwelled water masses on the shelf with potential impact on global carbon sequestration [7]. An analysis of the topography (Fig. 4) shows an approximately straight slope which increases linearly (at the rate of 0.0018 per meter) in the northward direction. We may transform our analytic coordinate systems into one consistent with the SAB by reversing the sense of y and expanding h about some distance ($y_0 \gg 1$) far from the singularity. At these large distances far from the singularity, the topography is approximated by one with a linearly increasing slope when looking towards the singularity (north in the case of the SAB), or linearly decreasing slope when looking away from the singularity (south in the case of the SAB). Such a linearly increasing/decreasing slope is consistent with the topography of the SAB, thus the form of the topography assumed in the above analytic formulation is expected to be a reasonable approximation to that of the SAB. Indeed, the right panel of Fig. 4 shows that the mean topographic slope measured along the SAB from the northernmost section to southernmost in a coordinate system with the singularity transformed to $y_0 = 175$ km and $\alpha = 125$ is an excellent fit to the topography of the region.

While most of the mathematical assumptions made in Section 3 are fairly standard and are expected to apply to the SAB, the assumptions of $L^2 \gg L_D^2$ and the existence of broad, weak northward flow should be justified. The numerical climatologies of Blanton et al. [16] show that a broad northward flow over the SAB develops in response to summer wind forcing. It is also shown that this broad flow is weak (<0.05 m/s) over the region of interest. In addition, summer is the stratified season on the SAB with observations showing a typical 10-15km internal radius of deformation [17,18]. Thus the assumptions of cross-slope length scale far exceeding the internal radius of deformation is also reasonable. Ultimately, we conclude that the above analytic solution is a reasonable idealized model for the summer stratified season over SAB. Assuming a current magnitude of approximately 0.05 m/s, a 75km shelf width of averaged depth 35 m, $L_D \approx$ 12.5km, $f \approx 7.6 \times 10^{-5}$, and $h_E \approx 10$ m, then $K_0 \approx 0.45$ for the SAB. For the well-mixed winter season (when wind-driven SAB flow is predominantly to the south), the barotropic linear solution of Kuehl [14] is applicable.

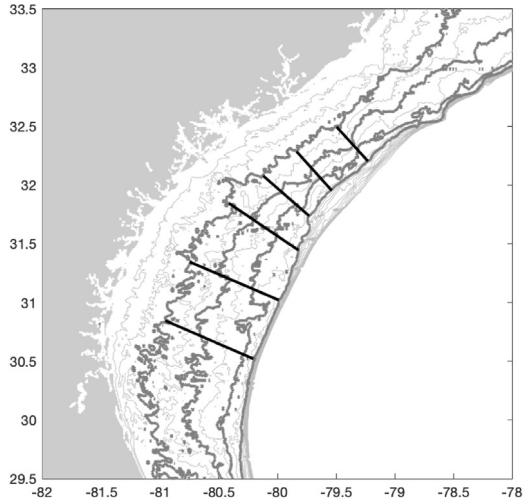

Fig. 3. Illustration of the SAB topography with representative cross-slope sections indicated by black lines. 20, 30, 40 and 50 m isobaths are indicated by thick gray lines with isobaths between 10 and 100 m indicated by light gray lines at 5 m intervals.

Fig. 5 show a realization of the analytic solution Eq. (13) to the SAB at the sections illustrated in Fig. 3 and with parameters indicated above. The vertical dashed lines represent the 25 m and 45 m isobaths, which become closer to each other as the topography steepens. Notice that as the flow moves northward, the 25 m and 45 m isobaths bracket transport between ≈ 0.1 and 0.9 (80% of the transport). This is consistent with the tendency of the analytic solution to follow isobaths. In addition to the flow structure, the increase in peak velocity as the flow moves north is seen in the right panel of Fig. 5. The topographic constriction has resulted in more than a doubling of the peak current speeds.

6. Final comment

We have not commented on the stability of this flow pattern, simply that such a steady base flow pattern exists. However, it is intriguing to compare this solution with the experimental and theoretical results of Nost et al. [19], which investigated cyclonic and anticyclonic flows in basins with sloping boundaries. Such results suggest the above analytic solution may be unstable. Though, the analysis of Nost et al. considered a flow pattern with branching streamline. Such branching, in conjunction with weak viscous effects, can lead to mismatches in information propagation along differing paths of the branching streamlines [20]. Such information mismatches lead to slight discontinuities

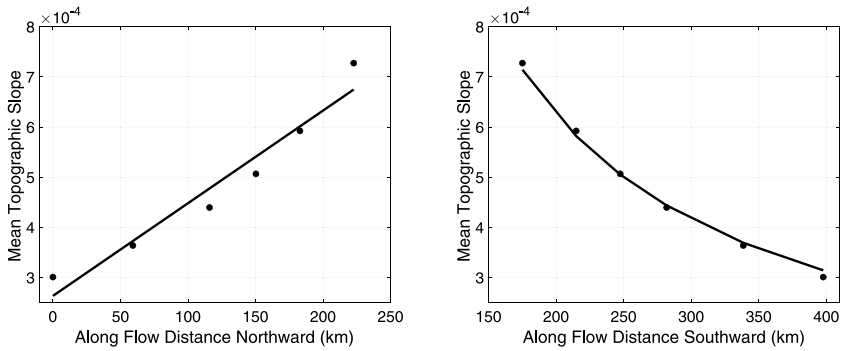

Fig. 4. (Left) Mean topographic slope (at sections indicated in Fig. 3) measured along the SAB from southernmost section to northernmost and linear trend line. Linear trend indicates an increasing slope at the rate of 0.0018/m with $R^2 = 0.94$. (Right) Dots are mean topographic slope (at sections indicated in Fig. 3) measured along the SAB from northernmost section to southernmost. Line is the topographic fit in a coordinate system with the singularity transformed to $y_0 = 175$ km with $\alpha = 125$.

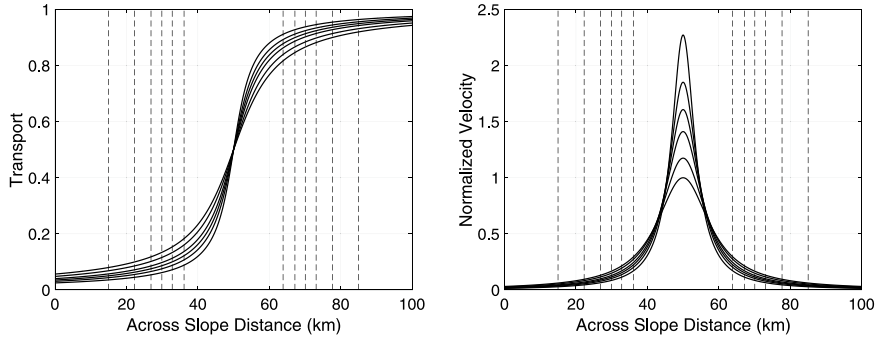

Fig. 5. (Left) Transport along the SAB at sections indicated in Fig. 3. The transport function steepens because the current is a compressing jet. The vertical dashed lines represent the 25 m and 45 m isobaths, which become closer to each other as the topography steepens. (Right) Normalized velocity along the SAB at sections indicated in Fig. 3. The peak velocity increases because the current is a compressing jet. Again, the vertical dashed lines represent the 25 m and 45 m isobaths, which become closer to each other as the topography steepens.

in transport (that physically manifest as jets) if/when the streamlines reconnect, which generate non-intuitive flow patterns. Thus, the question of stability remains unknown and is a promising direction for future research.

Declaration of competing interest

The authors declare that they have no known competing financial interests or personal relationships that could have appeared to influence the work reported in this paper.

Acknowledgment

The authors are thankful to the National Science Foundation, USA for funding this research via grant number 1823452.

References

[1] H. Blasius, Frenzschichten in Flüssigkeiten mit kleiner Reibung, Z. Angew. Math. Phys. 56 (1908) 1–37.
[2] V.W. Ekman, On the influence of the earth's rotation on ocean-currents, Ark. Mat. Astr. Fys. 2 (11) (1905) 1–52.
[3] R.H. Weisberg, L. Zheng, E. Peebles, Gag grouper larvae pathways on the West Florida Shelf, Cont. Shelf Res. 88 (2014) http://dx.doi.org/10.1016/j.csr.2014.06.003.
[4] R.H. Weisberg, L. Zheng, Y. Liu, Basic tenets for coastal ocean ecosystems monitoring: A west Florida perspective, coastal ocean observing systems, in: Y. Liu, et al. (Eds.), Coastal Ocean Observing Systems, Elsevier, London, U.K., 2015, pp. 40–57, http://dx.doi.org/10.1016/B978-0-12-802022-7.00004-3.
[5] R.H. Weisberg, L. Zheng, Y. Liu, West Florida Shelf upwelling: Origins and pathways, J. Geophys. Res. Oceans 121 (2016) 5501–5515, http://dx.doi.org/10.1002/2015JC011384.
[6] G.-A. Paffenhofer, B.K. Sherman, T.N. Lee, Summer upwelling on the southeastern continental shelf of the U.S.A. during 1981. Abundance, distribution and patch formation of zooplankton, Prog. Oceanogr. 19 (1987) 403–436.
[7] D.K. Savidge, W.B. Savidge, Seasonal export of South Atlantic Bight and Mid-Atlantic Bight shelf waters at cape hatteras, Cont. Shelf Res. 74 (2014) 50–59.
[8] L. Zavala Sanson, G.J. van Heijst, Ekman effects in a rotating flow over bottom topography, J. Fluid Mech. 471 (2002) 239–255.
[9] J. Pedlosky, Geophysical Fluid Dynamics, Springer, 1987.
[10] B. Cushman-Roisin, Introduction to Geophysical Fluid Dynamics, Prentice-Hall Inc, 1994.
[11] J.J. Kuehl, V.A. Sheremet, Two-layer gap-leaping oceanic boundary currents: experimental investigation, J. Fluid Mech. 740 (2014) 97–113.
[12] V.A. Sheremet, J. Kuehl, Gap leaping western boundary current in a circular tank model, J. Phys. Oceanogr. 37 (2007) 1488–1495.
[13] G.T. Csanady, The arrested topographic wave, J. Phys. Oceanogr. 8 (1978) 47–62.
[14] J.J. Kuehl, An analytic solution for barotropic flow along a variable slope topography, Geophys. Res. Lett. 41 (2014) http://dx.doi.org/10.1002/2014GL061188.
[15] R. Ibanez, J. Kuehl, K. Shrestha, W. Anderson, A nonlinear self-similar solution to barotropic flow over rapidly varying topography, Nonlinear Process. Geophys. 25 (2018) 201–205.
[16] B.O. Blanton, A. Aretxabaleta, F.E. Werner, H.E. Seim, Monthly climatology of the continental shelf waters of the South Atlantic Bight, J. Geophys. Res. 108 (2003) http://dx.doi.org/10.1029/JC001609.
[17] T.N. Lee, J.A. Yoder, L.P. Atkinson, Gulf stream frontal eddy influence on productivity of the southeastern U.S. continental shelf, J. Geophys. Res. 96 (C12) (1991) 22191–22205.
[18] D.W. Menzel (Ed.), Ocean Processes: U.S. Southeast Continental Shelf, US Department of Energy, Washington, DC, 1993, p. 112.
[19] O.A. Nost, J. Nilsson, J. Nycander, On the asymmetry between cyclonic and anticyclonic flow in basins with sloping boundaries, J. Phys. Oceanogr. 38 (2008) 771–787.
[20] J.J. Kuehl, V.A. Sheremet, Experimental investigation of shelf flow crossing over a strait, J. Phys. Oceanogr. (2020) Under Revision.